

Quark/gluon jet discrimination at HERA

Jon Pumplin¹

Department of Physics and Astronomy, Michigan State University, East Lansing, MI 48824, USA
and

Deutsches Elektronen-Synchrotron DESY, Notkestrasse 85, D-2000 Hamburg 52, Germany

Received 14 July 1992

(Revised 5 October 1992)

Accepted for publication 12 November 1992

Tests of QCD, and its representation by Monte Carlo shower models such as PYTHIA or HERWIG, are proposed for low- Q^2 events at the e^-p collider HERA. The tests are based on observable features that distinguish between quark jets and gluon jets. They therefore provide sensitivity to the description of parton branching, and to the parton distributions in the photon and proton.

1. Introduction

Large momentum transfer interactions in e^+e^- , e^-p , and $\bar{p}p$ scattering are characterized by the production of hadronic jets, which result from the underlying production of quarks and gluons. The production and hadronization of the jets is described by Monte Carlo shower models [1,2], which contain a mixture of perturbative and leading-log QCD theory, and non-perturbative phenomenology.

Using the shower model HERWIG [1] to simulate $\bar{p}p$ scattering, I have previously shown that the quark or gluon origin of a jet can be recognized on a probabilistic basis by the use of certain variables which characterize the internal “shape” of the jet [3]. (Here as elsewhere in this paper, antiquarks are included along with quarks since there is no hope in general to discriminate between q and \bar{q} jets.) Other methods for quark/gluon jet discrimination that are generally less effective have also been described [4–7]. All of these methods are based on the fundamental physics that gluons branch ($G \rightarrow GG, q\bar{q}$) more readily than quarks ($q \rightarrow qG$). For example gluon emission from a gluon is stronger than gluon emission from a quark by a factor $9/4$ in lowest-order perturbation theory.

The purpose of the present paper is to extend the previous studies to e^-p scattering, where the possibility will soon exist to compare with experimental

¹ Bitnet: PUMPLIN@MSUPA

data from HERA at $\sqrt{s} = 314 \text{ GeV}$. In order to make this study as independent as possible from my previous ones, I use the Monte Carlo program PYTHIA [2] this time in place of HERWIG [1]. I also use a different jet definition algorithm, and work at the somewhat lower jet E_T 's appropriate for HERA. The overall agreement with the previous work shows that the predictions are robust.

Because of the photon propagator, the majority of moderately high E_T jets in e^-p scattering are produced by almost-real ($low-Q^2$) photon exchange. The scattered electron comes out at a very small angle and generally goes undetected. This study deals mainly with these events, which are favorable for study at the lower luminosities that will be available in early running at HERA.

This work is directed toward testing the combination of QCD theory and phenomenology contained in the shower Monte Carlos against experiment, in a way that is sensitive to the relative amounts of q- and G-jets produced, along with the systematics of jet development. The variables I use are good at distinguishing between the two kinds of jets. They are therefore sensitive to the amount of branching, and hence test especially that aspect of a shower model, along with testing the prediction for the q/G production ratio.

According to the Monte Carlo, the ratio q/G varies with jet pseudorapidity η_j . This offers one possibility to test the separation technique experimentally. A second possible test can be made by comparing with deep-inelastic (DIS) events in which the scattered electron is detected. In these events, the hadronic jet is essentially always a quark jet.

A more distant goal of this work is to use the probabilistic tagging of q- or G-jets as an aid to measuring parton distributions, especially of the photon. Another potential application is to jet spectroscopy, where it would be useful for observing $W \rightarrow$ jets for example [3,8].

2. Event simulation and cuts

Simulated events of e^-p scattering at HERA energy (30 GeV electrons on 820 GeV protons) were generated using PYTHIA 5.6 [2], which has been found to describe jets observed in Z^0 decay at LEP rather accurately [9,10]. The parameters used were the default settings for photoproduction, in which the scattered electron is not detected. Among the default choices are structure functions of Drees and Grassie [11] for the photon, and EHLQ1 for the proton. All relevant two-body hard scattering processes were included: "unresolved photoproduction" ($\gamma q \rightarrow Gq$, $\gamma G \rightarrow q\bar{q}$) and "resolved photoproduction" ($qq \rightarrow qq$, $q\bar{q} \rightarrow q\bar{q}$, $q\bar{q} \rightarrow GG$, $GG \rightarrow q\bar{q}$, $Gq \rightarrow Gq$), along with their charge-conjugate processes. Hard scattering with a heavy quark in the initial state or a γ in the final state was found to be negligible with our kinematical cuts. On the other hand, heavy quarks in the final state were included and make important contri-

butions: $\sim 24\%$ for c and $\sim 4\%$ for b. From the standpoint of jet shape, they are not importantly different from u, d, or s.

Jets were identified using a modified version of the subroutine LUCCELL, whose original form comes with the JETSET 7.3 part of the PYTHIA package. LUCCELL uses an idealized segmented calorimeter detector, consisting of cells which I have set to width 0.100 in pseudorapidity η ($= -\ln \tan \theta/2$ in the laboratory frame) by 0.098 in azimuthal angle ϕ . The input information to LUCCELL consists of the total transverse energies in each of these cells. Jets are found by summing E_T over all cells within a cone $[(\eta - \eta_J)^2 + (\phi - \phi_J)^2]^{1/2} < 0.8$. The axis (η_J, ϕ_J) of the cone is initially found by trying the direction of every unassigned cell that has $E_T > 1.5$ GeV. An improved jet axis is defined by the E_T -weighted average over cells in the cone. *LUCCELL was modified to iterate this procedure, so that the assignment of cells to the jet is made consistent with the final jet axis.*

Events were kept only if the modified LUCCELL jet-finder found two jets. The jets were required to contain more than one particle, to eliminate a small fraction of events in which an apparent “jet” was actually a scattered electron. Such deep inelastic scattering (DIS) events will be discussed separately below. A cut $|\eta_J| < 2.7$ was imposed to avoid the extreme forward and backward directions which are experimentally inaccessible. In order to emphasize two-jet physics, the axes of the two jets were required to be back-to-back in ϕ_J within $\pm 29^\circ$, and their observed energies were required to be approximately equal:

$$|E_T^{(1)} - E_T^{(2)}| < [E_T^{(1)} E_T^{(2)}]^{1/4} \quad (1)$$

in GeV = 1 units. (A cut on the magnitude of the sum of the two jet transverse momentum *vectors* in place of the last two cuts would have been similar and perhaps slightly more to the point.) There is no ambiguity in associating the momentum vectors of the jets that survive these cuts with those of the hard-scattered partons in the Monte Carlo, and thereby identifying the q or G parentage of the jets.

To study the features of the jets, cuts $E_T > 12, 24, \text{ or } 48$ GeV were imposed on the observed jet transverse energy. The corresponding cross sections are shown in table 1, along with the percentages contributed by the most important underlying hard-scattering processes. The cross section falls rather rapidly with E_T , so the events in each category have an average E_T that is not far above the minimum. The highest E_T region will require considerable running time at HERA, but it is worth the effort in part because it will allow fuller comparison with jets produced in e^+e^- scattering at LEP and in $\bar{p}p$ at the TEVATRON.

In order to avoid bias in generating the events, it is necessary to allow broad ranges in p_T^{hard} ($> 5, > 10, \text{ and } > 20$ GeV respectively) for the $2 \rightarrow 2$ hard scattering in PYTHIA. This can be seen in fig. 1, where the main peak of the distribution in p_T^{hard} is close to the observed jet E_T , but there is a tail extending

TABLE 1

Cross sections for quark jets (σ_q) and gluon jets (σ_G) from two-jet events, and quark jets (σ_{DIS}) from deep inelastic scattering. The major hard-scattering contributors to the two-jet cross sections are also listed.

	$E_T^{\text{jet}} > 12 \text{ GeV}$	$E_T^{\text{jet}} > 24 \text{ GeV}$	$E_T^{\text{jet}} > 48 \text{ GeV}$
σ_q	3164 pb	179 pb	3.7 pb
$\gamma G \rightarrow q\bar{q}$	46.3%	45.9%	39.3%
$qG \rightarrow qG$	25.4%	17.6%	8.0%
$qq \rightarrow qq$	19.1%	22.0%	23.2%
$\gamma q \rightarrow Gq$	7.5%	13.2%	28.4%
σ_G	1619 pb	66 pb	1.4 pb
$qG \rightarrow qG$	50.4%	47.4%	21.5%
$GG \rightarrow GG$	35.7%	17.9%	3.8%
$\gamma q \rightarrow Gq$	13.3%	33.9%	73.5%
σ_{DIS}	1520 pb	201 pb	21 pb

to small p_T^{hard} that presumably reflects initial state radiation. This point was overlooked in the event generation of ref. [7].

Table 1 shows that the relative importance of the various $2 \rightarrow 2$ hard scattering processes varies considerably with jet E_T . Testing the q/G ratio will therefore test the QCD jet production theory in a highly non-trivial way.

Table 1 also shows the cross section for DIS events in which a scattered electron is required to play the role of a jet to satisfy the two-jet cuts. Events of this type will be easily distinguished from events in which both jets are hadronic. They can be used as a sample of essentially pure quark jets. The DIS cross sections are seen to be somewhat smaller than the low- Q^2 two-jet cross sections at low E_T , but considerably larger at large E_T . (The DIS cross sections given here are approximate, since the DIS theory used by PYTHIA presumably assumes $Q^2 \ll E_T^2$.)

3. Quark/gluon jet discrimination

We wish to look at features that are internal to the observed jet, i.e. that are based only on the particles within the jet cone. Four variables for distinguishing between quark jets and gluon jets were found particularly useful in previous studies, and have been found again to be successful here. A new jet discrimination variable, which is related to the theoretically interesting dependence of jet E_T on cone size [12], has also been found useful.

The first three variables use only the E_T deposited in each 0.1×0.1 calorimeter cell as input information. In computing these variables, *all cells with $E_T < 100 \text{ MeV}$ were ignored*. The remaining two variables make full use of the momenta of the final-state particles.

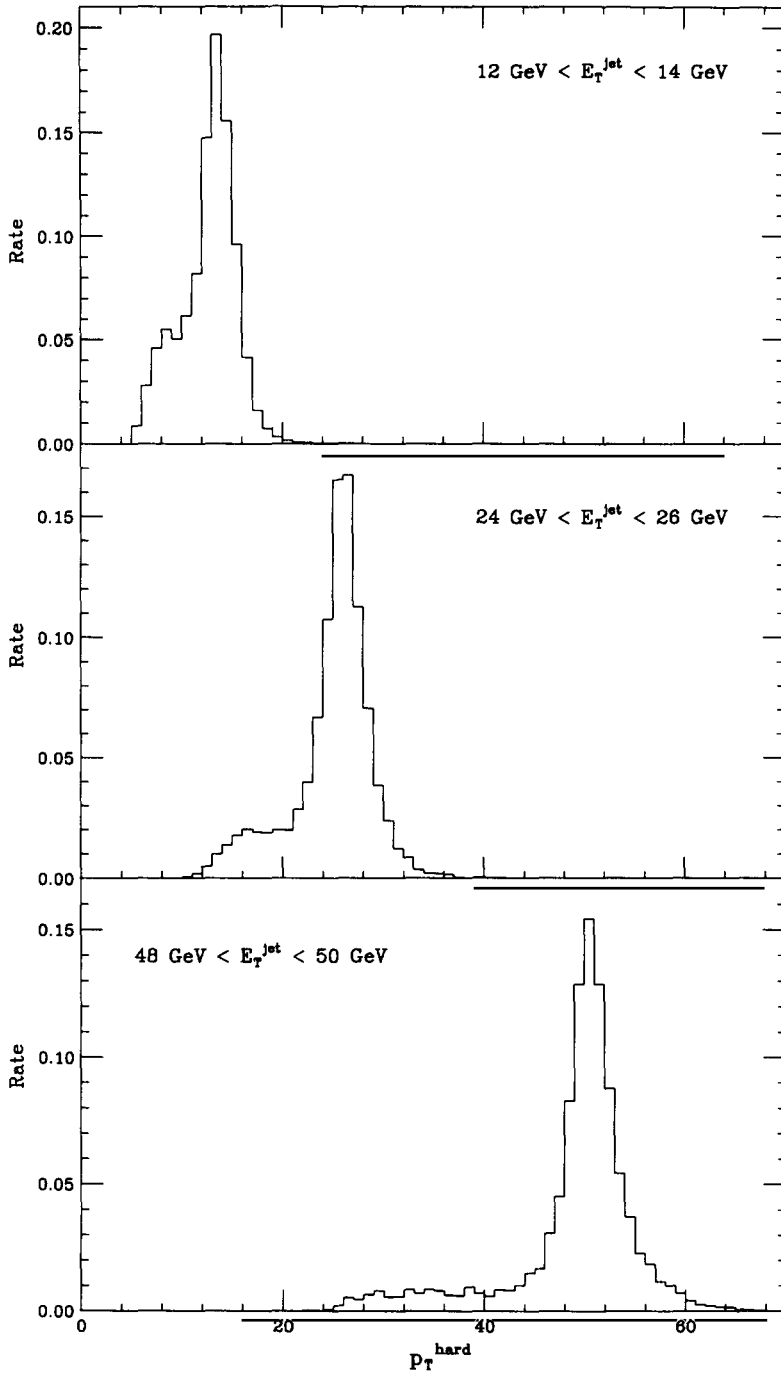


Fig. 1. Histogram of the transverse momentum p_T^{hard} of the underlying hard scattering, for jets with specific values of observed E_T .

(1) N_X is defined by adding up the E_T 's of all cells within the jet cone; then adding them up again in descending order of E_T and counting the number N_X of cells necessary to include all but $X\sqrt{E_T}$ of the total. Here I use $X = 0.5 \text{ GeV}^{1/2}$. N_X can be assigned a fractional part by interpolating to handle the last partial cell, but that is not essential — particularly if a bin width of 1 is used.

(2) S is defined as the mean squared radius of the jet in (η, ϕ) space. Specifically,

$$S = \left\langle (\eta - \eta_J)^2 + (\phi - \phi_J)^2 \right\rangle, \quad (2)$$

where $\eta_J = \langle \eta \rangle$, $\phi_J = \langle \phi \rangle$, and $\langle \dots \rangle$ is defined as the E_T -weighted average over cells inside the jet cone.

(3) N_{cells} is defined as simply the number of calorimeter cells with $E_T > 100 \text{ MeV}$ inside the jet cone.

(4) $N_{\text{particles}}$ is defined as the total number of final particles within the jet cone. (This was done without subtlety: π^0 's were counted as two, for example, because they appear as two photons. Using the charged multiplicity instead leads to similar results, however.)

(5) r_X is defined as the radius of a “small” cone that contains all but $X\sqrt{E_T}$ of the total E_T in the original cone. This variable is similar in spirit to N_X , and I again choose $X = 0.5 \text{ GeV}^{1/2}$. (As the cone radius is reduced, it seems natural to continually adjust the axis according to the E_T -weighted average of particles within the current cone. Just keeping the original axis fixed leads to nearly identical results, however.)

All five of these variables show significant differences between quarks and gluons, as shown in figs. 2–6. Each distribution peaks at a larger value for gluons than for quarks, as expected from the stronger branching of gluons in QCD. The differences shown will allow one to discriminate between quarks and gluons on a probabilistic basis: according to any one of the variables, some jets can be identified as very likely q, while others are very likely G, and still others are more or less ambiguous.

A special advantage of the discrimination variable N_X can be seen in fig. 2: the point at which the q- and G-curves intersect is only mildly dependent on jet E_T . This is in contrast to the E_T -dependence of cross-over points for the other variables seen in figs. 3–6. It means that N_X is especially well suited to q/G discrimination in samples of jets containing a broad range of E_T .

The quark/gluon differences appearing in figs. 2–6 can be quantified in the following manner. First imagine applying a cut $N_X \leq 5$ in fig. 2. By integrating the histogram over that region of N_X , this cut is found to preserve a fraction $F_q = 0.43$ of the quarks and a fraction $F_G = 0.11$ of the gluons. (If one is particularly interested in quarks, for example, one says that the cut has an efficiency $F_q = 43\%$ and that it suppresses the background/signal ratio by $F_G/F_q = 0.25$.) Different choices for the cut in N_X lead to different pairs (F_q, F_G) . The results

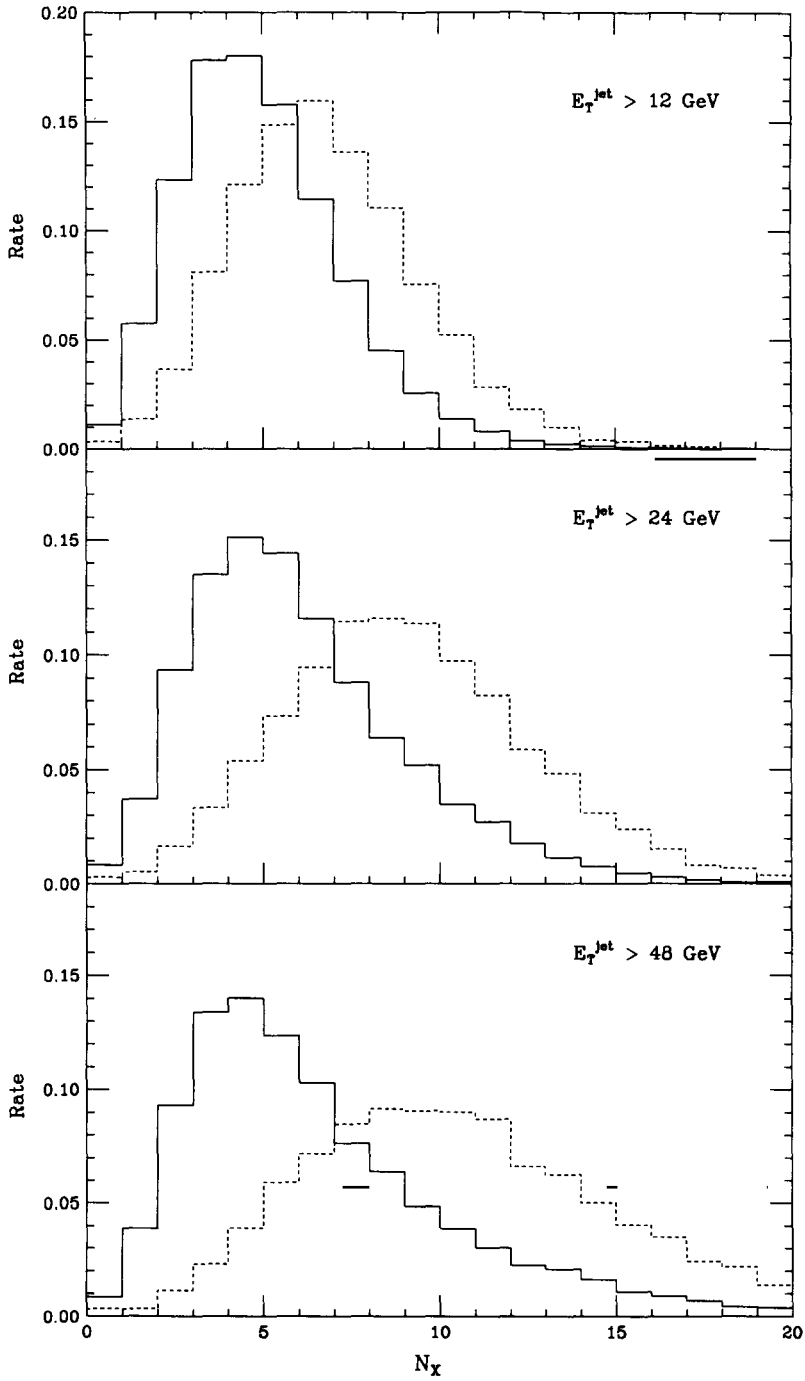


Fig. 2. Histograms of the q/G discrimination variable N_χ the number of calorimeter cells needed to include all but $0.5\sqrt{E_T}$ of the total jet E_T : quarks (solid), gluons (dashed). Each distribution is normalized to unit probability.

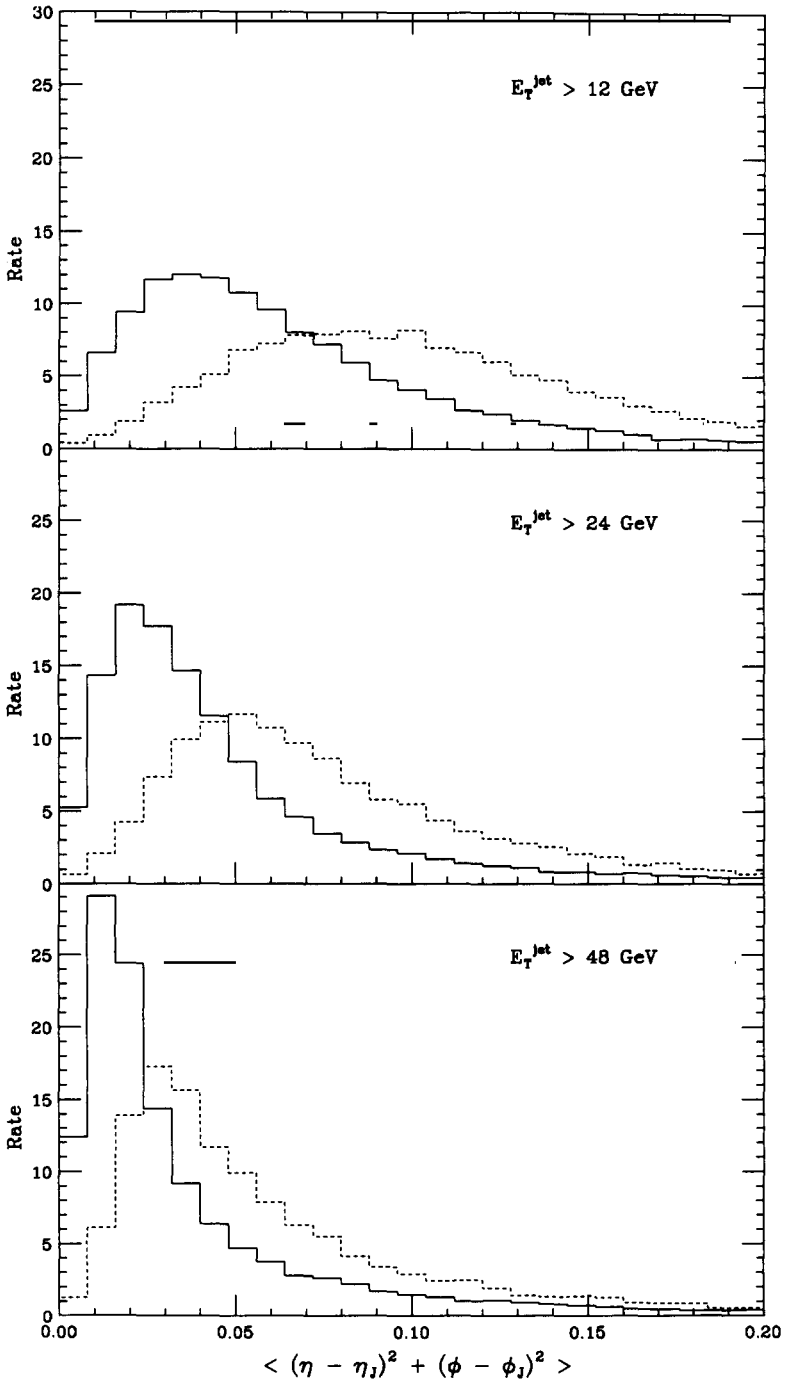


Fig. 3. Similar to fig. 2, for $S = \langle (\eta - \eta_j)^2 + (\phi - \phi_j)^2 \rangle$.

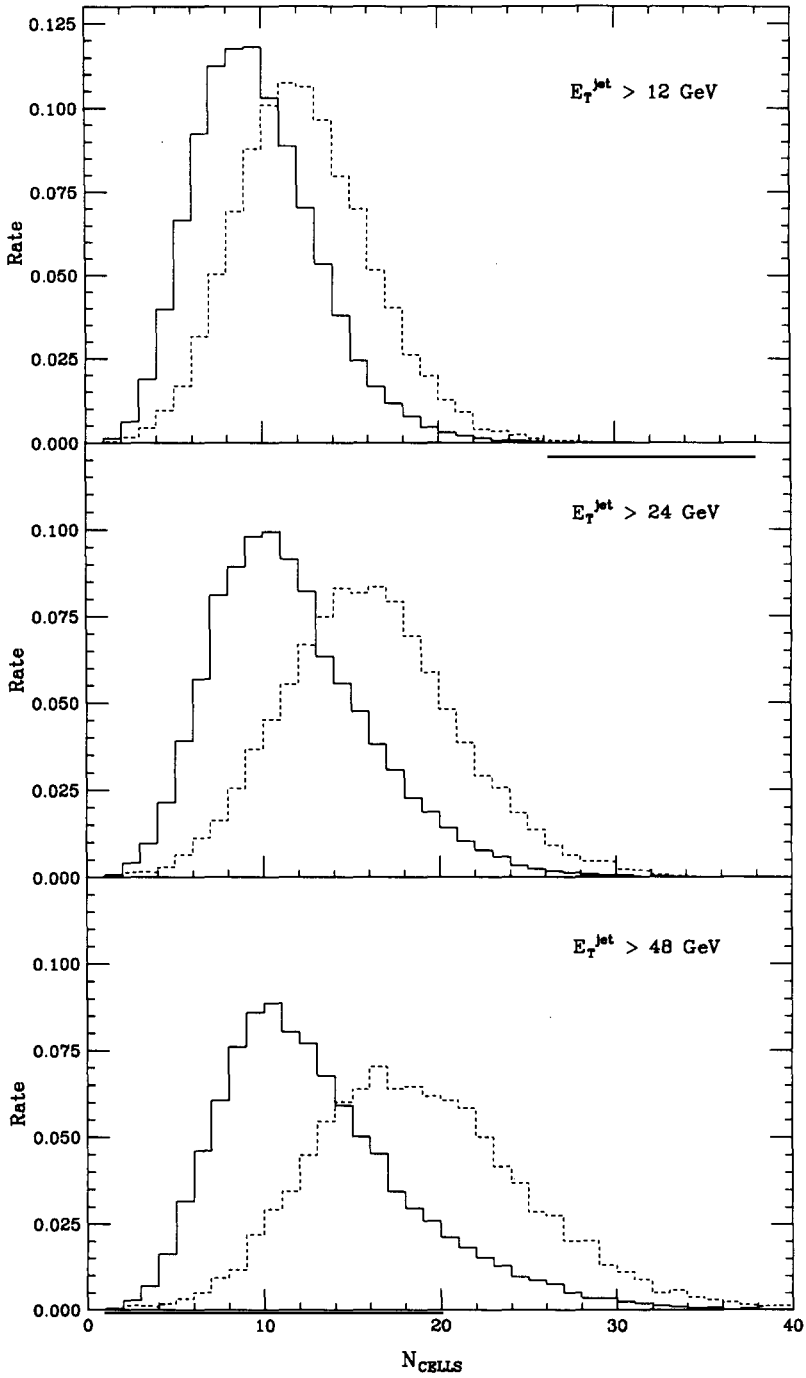


Fig. 4. Similar to fig. 2, for N_{cells} the number of 0.1×0.1 calorimeter cells in the jet cone with $E_T > 100 \text{ MeV}$.

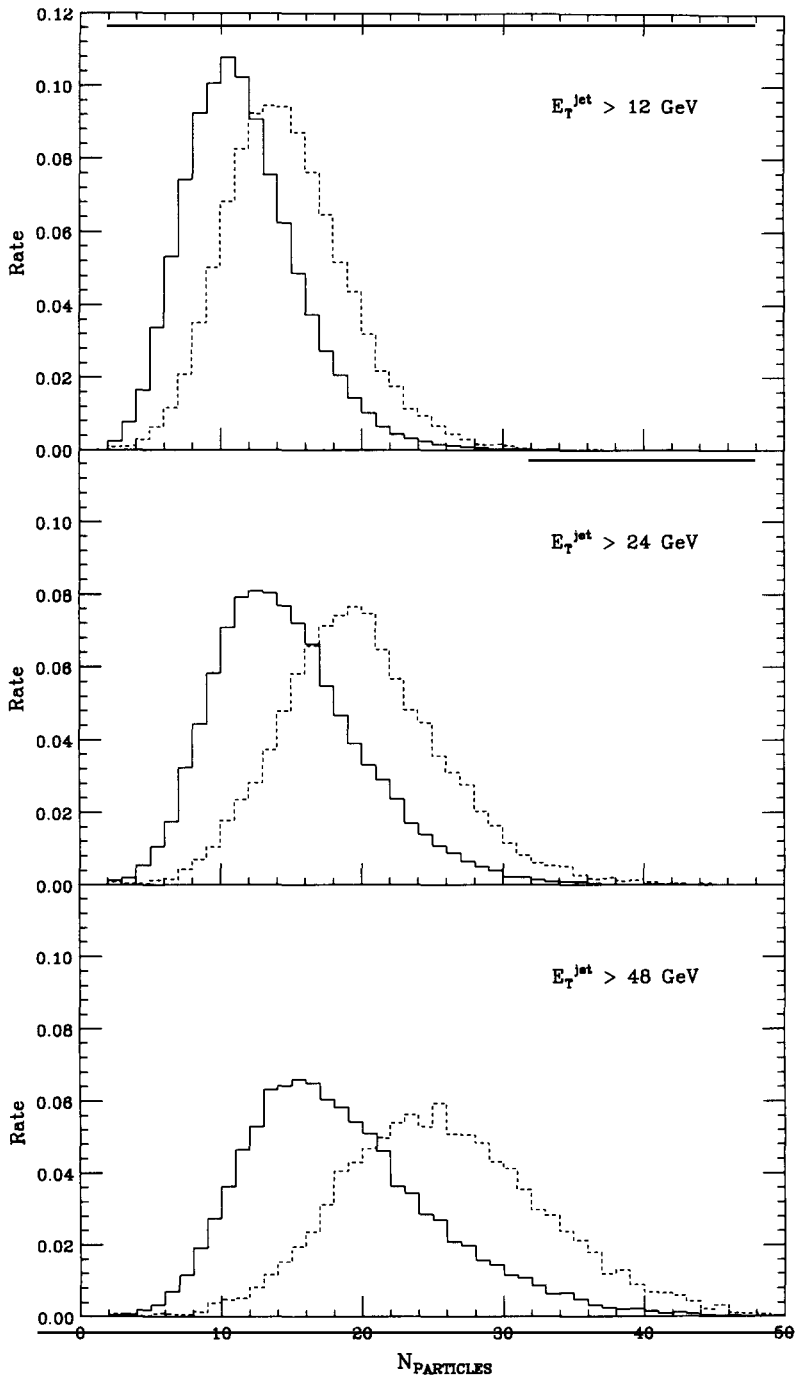


Fig. 5. Similar to fig. 2, for $N_{\text{particles}}$ the number of final particles within the jet cone.

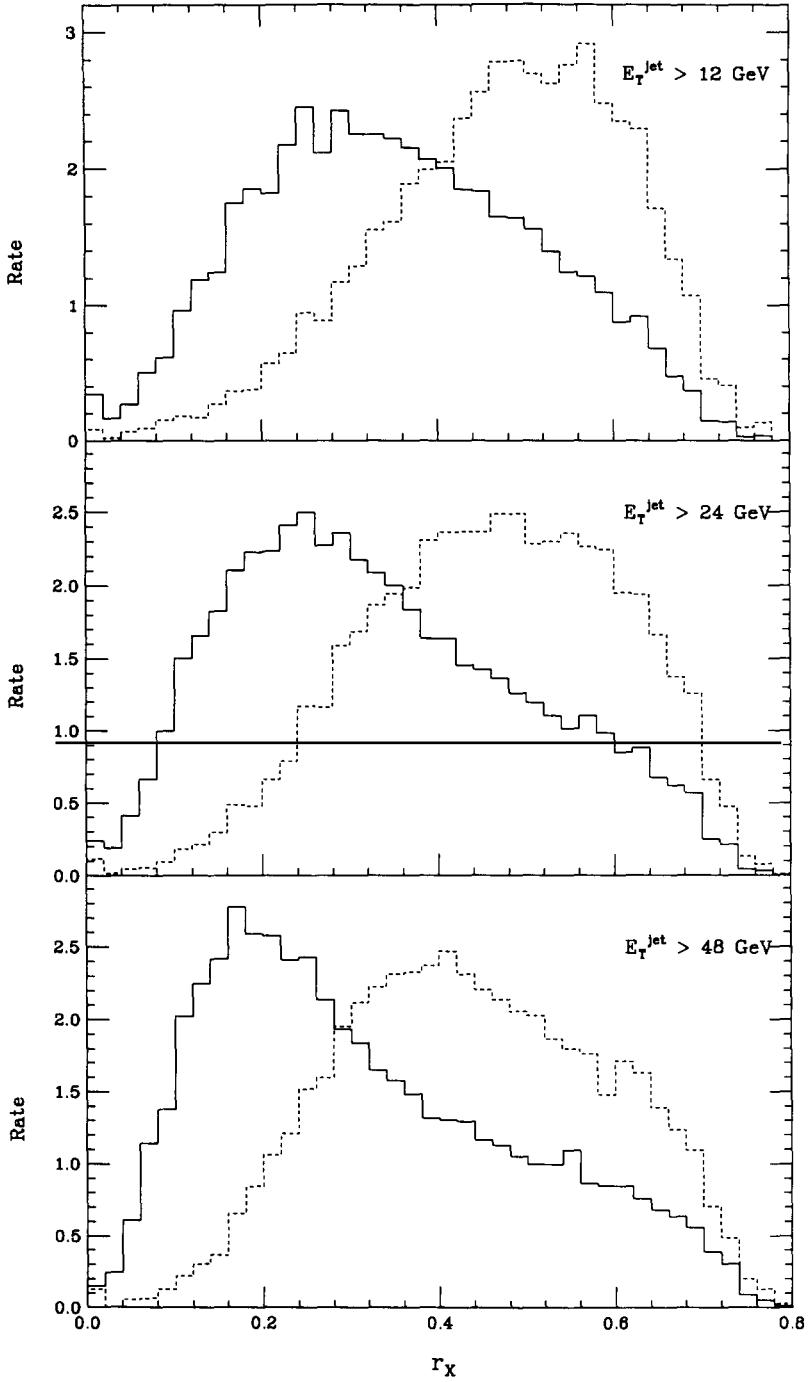


Fig. 6. Similar to fig. 2, for r_χ the radius of a cone that contains all but $0.5\sqrt{E_T}$ of the total jet E_T .

of all possible cuts in N_X can be displayed in a *discrimination graph* of F_q versus F_G . This graph completely characterizes the ability to distinguish quarks from gluons by means of the variable N_X^* .

Discrimination graphs are shown in fig. 7 for each of the five variables in each of three regions of jet E_T . The quality of discrimination is represented by the deviation of the curves from the diagonal line $F_q = F_G$ that would represent no discrimination at all. One sees that each variable provides a good deal of discrimination, with relatively small differences in quality between the variables, especially for $F_q < 0.5$. In more detail, N_X and the very simple variable N_{cells} are almost equally effective — so much so that they are both represented in fig. 7 by solid curves which are mostly unresolved. $N_{\text{particles}}$ is about equally good, while $\langle (\eta - \eta_J)^2 + (\phi - \phi_J)^2 \rangle$ is slightly better at $E_T \sim 12$ GeV and slightly worse at $E_T \sim 48$ GeV. r_X is similarly good at small F_q , especially at low E_T , but becomes ineffective at larger F_q .

Fig. 7 also shows that the q/G discrimination is better at small F_q : *it is easier to recognize quarks than gluons*. For example at $E_T^{\text{jet}} > 48$ GeV, to select quarks with an efficiency of 20%, one can obtain $F_q = 0.20$ and $F_G = 0.026$ (via the cut $N_X < 3.5$). This keeps 20% of the quarks while suppressing the gluons by a factor $F_G/F_q = 0.13$. On the other hand, to select gluons with that efficiency, one can obtain $F_G = 0.20$ and $F_q = 0.048$ (via the cut $N_X > 14.5$). This keeps 20% of the gluons while suppressing the quarks by only a factor $F_q/F_G = 0.24$.

The five q/G discrimination variables are fairly strongly correlated, as one could see from scatter plots. The correlation is by no means complete however. As a specific example, at $E_T^{\text{jet}} > 24$ GeV the cuts $N_X < 6.2$ and $N_{\text{cells}} \leq 11$ each keep 58.9% of quarks and 19.7% of gluons. These cuts do not keep exactly the same events, for only 53.6% of q and 16.1% of G pass both of them. (One might imagine that better discrimination could be obtained by requiring both cuts, but the truth is that a tighter cut on N_X alone yields a smaller F_G for the same F_q . There does not seem to be any way to combine two or more of the above variables into a single “super-variable” which works much better than any one of them alone. A number of attempts to make use of charge patterns among the leading particles in the jet also led to nothing valuable for q/G discrimination. This agrees with the result of ref. [13].)

Fig. 8 shows the discriminative ability of N_X for the three E_T ranges of fig. 7 on a single plot. It shows that the ability to distinguish between quarks and gluons improves with increasing jet E_T .

Fig. 8 also shows the N_X discrimination found in a previous study [3] for jets with $40 < E_T < 60$ GeV. This curve was obtained for $\bar{p}p$ scattering at $\sqrt{s} = 1800$ GeV instead of e^-p scattering at $\sqrt{s} = 314$ GeV, using a more elaborate

* This method for comparing two histograms is useful in many contexts, and should be made easily available in general software tools for the analysis of histograms!

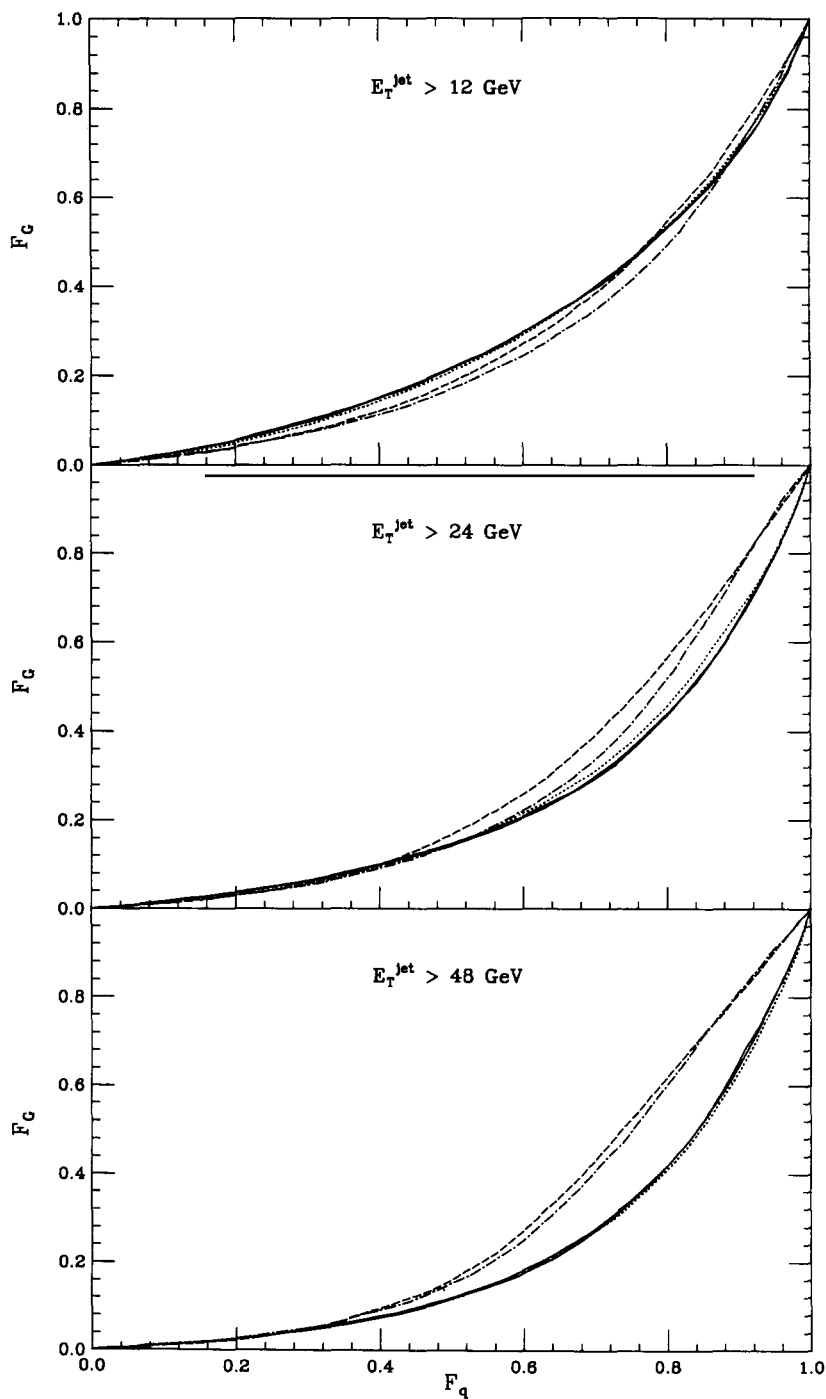


Fig. 7. "Discrimination graph" which displays the effectiveness of each quark/gluon discrimination variable: N_χ (solid), N_{cells} (solid), $N_{\text{particles}}$ (dotted), $\langle(\eta - \eta_j)^2 + (\phi - \phi_j)^2\rangle$ (dot-dash) and r_χ (dashed).

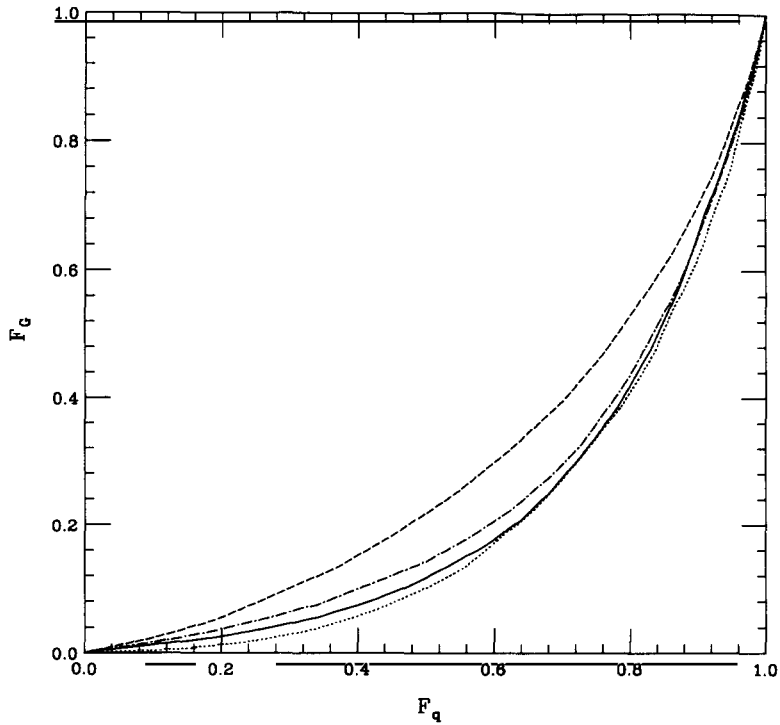


Fig. 8. “Discrimination graph” for the variable N_X in various E_T^{jet} ranges: $E_T^{\text{jet}} > 12$ GeV (dashed), $E_T^{\text{jet}} > 24$ GeV (dot-dash), $E_T^{\text{jet}} > 48$ GeV (solid). The dotted curve is from $E_T^{\text{jet}} = 40 - 60$ GeV jets obtained using HERWIG for pp scattering at $\sqrt{s} = 1800$ GeV [3].

jet-finder, and using the simulation program HERWIG instead of PYTHIA. *The approximate agreement with the $E_T > 48$ GeV curve therefore supports the consistency and universality of our discrimination procedure.* At small F_q , which corresponds to small N_X , one can see however that the previous study predicts somewhat larger differences between q-jets and G-jets. This may reflect intrinsic differences [9,14] between HERWIG and PYTHIA.

4. Experimental tests

Studying quark/gluon discrimination with Monte Carlo events is relatively easy, because the true q- or G-identity of the parent of each jet is known in the simulation. Testing against experiment is another matter. One possibility is to obtain independently tagged samples of quark jets and gluon jets by observing electrons or muons that appear as a result of weak decays in b- and c-jets [10]. This has been applied to $e^+e^- \rightarrow$ three-jet events, along with the assumption

that the softest jet comes from a gluon [10,15]*.

Here I propose a different method for testing quark/gluon identification, which is convenient for HERA data. The method is based on the different pseudorapidity dependence of quark and gluon jet production. Predicted η_J distributions are shown in fig. 9 for jets from the two-jet events that pass our cuts. Note that positive η_J is favored because the energy of the initial proton is much larger than that of the initial electron at HERA.

To make a specific experimental proposal, consider the $E_T > 12$ GeV jet sample. The 25% of these jets having the lowest η_J ($\eta_J < 0.4$) contains 19% gluons according to the simulation. Distributions from this sample can be compared with those from the 25% of jets having the highest η_J ($\eta_J > 1.9$). That sample contains 47% gluons according to the simulation. The gluon fractions in these two η -regions are sufficiently different that the intrinsic quark/gluon differences should be observable. This is shown in fig. 10 for N_X .

Similarly for the $E_T > 24$ GeV jet sample: the 25% of jets with lowest η_J ($\eta_J < 0.6$) contains 14% gluons, while the 25% with highest η_J ($\eta_J > 1.8$) contains 38% gluons. The N_X distributions corresponding to these cuts also show a clear difference in fig. 10. It will be interesting to look for these differences, and the corresponding differences for the other variables of sect. 3 experimentally. *This is the essential experimental proposal of this paper.* A quantitative method to analyze the differences would be to compare the histograms from the two extreme η_J -regions using discrimination graphs analogous to fig. 7. The distributions in N_X and the other variables without η -cuts are of course important to measure also, since they are sensitive to the overall q/G ratio and to the overall amount of branching in the development of QCD showers.

A further possible experimental test would be to use DIS events in which a deeply-inelastic scattered electron is observed and the associated high E_T jet presumably began as a quark. One could even parametrize the distribution in a particular variable such as N_X separately for q and G, and fit the three jet samples (low η , high η , DIS) to measure the gluon fraction in the low- η and high- η regions. The assumption that the average behavior of quark jets and gluon jets does not vary with η , and that the characteristics of quark jets from two-jet events are the same as those from DIS is crucial to this and to the above experimental tests. I have verified these assumptions using the simulation.

In this paper, high- E_T jets have been studied one at a time. Further work could be done by applying the q/G discrimination variables to both jets in the two-jet events simultaneously. One could thereby hope to measure individual cross

* A study [10] of this type at LEP found only small differences in charged-particle multiplicities between q- and G-jets, which would seem to be in conflict with our results in fig. 5. However, the experimental data are consistent with a PYTHIA simulation that includes the tagging procedure and a detector simulation, so there is no experimental reason to doubt our results, which are also based on PYTHIA.

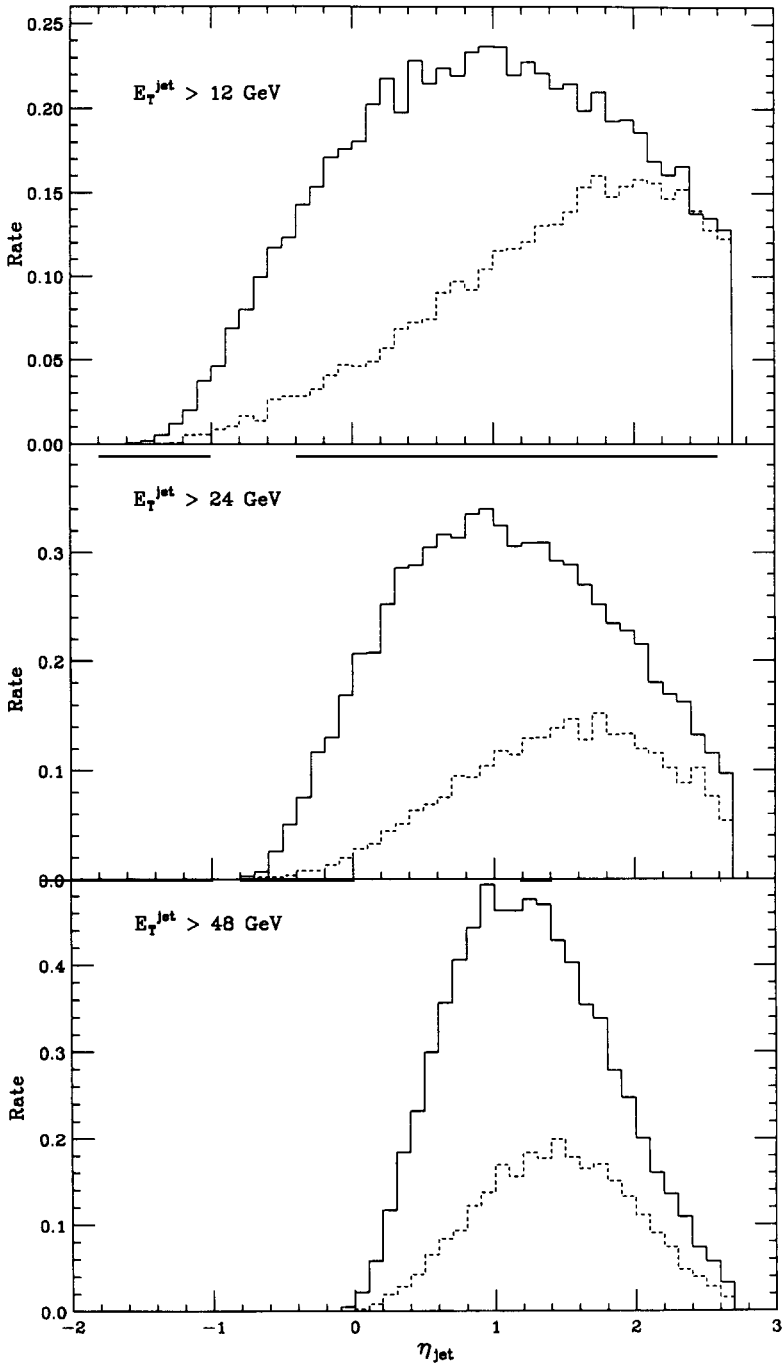


Fig. 9. Cross sections for quark jets (solid) and gluon jets (dashed), with correct relative normalization, as a function of pseudorapidity.

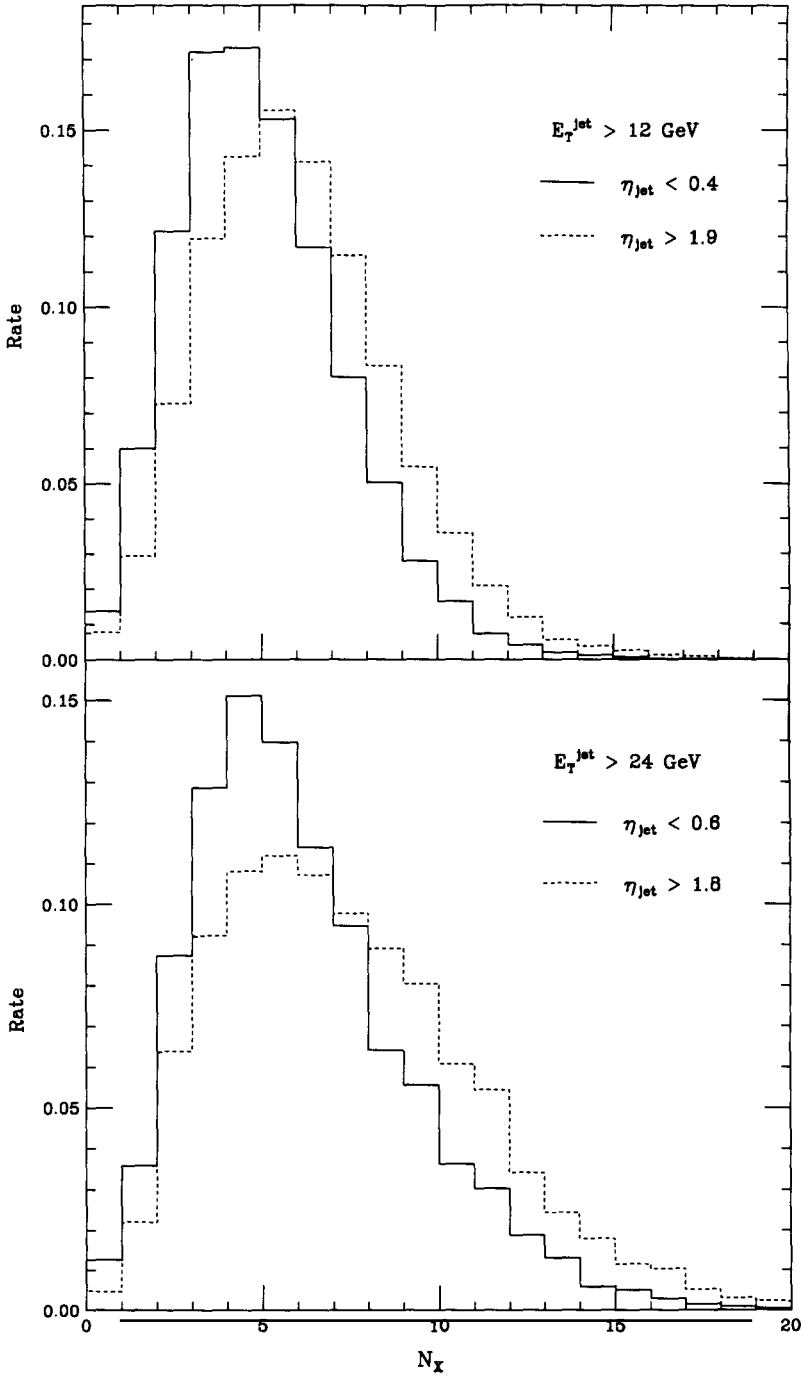


Fig. 10. Predicted N_X distributions (q and G combined) in the presence of cuts on η_j which suppress (solid) or enhance (dashed) the fraction of gluons. Each distribution is normalized to unit probability.

sections for each of the possible final-state categories $qq + q\bar{q} + q\bar{q}$, $Gq + G\bar{q}$, and GG . A further classification of the final states could be made according to the presence or absence of a hadronic remnant jet in the electron direction, which signals a “resolved” or “unresolved” photon process [16].

I thank D. Monaldi and S. Ellis for useful and interesting discussions, S. Bethke and J. W. Gary for information about the OPAL results, and DESY for supporting my sabbatical visit.

References

- [1] G. Marchesini, B. Webber, G. Abbiendi, I. Knowles, M. Seymour and L. Stanco, HERWIG Version 5.4 (January 1992), *Comput. Phys. Commun.* 67 (1992) 465
- [2] H.-U. Bengtsson and T. Sjöstrand, *Comput. Phys. Commun.* 46 (1987) 43; PYTHIA 5.6 manual; JETSET 7.3 manual;
T. Sjöstrand, PYTHIA at HERA, CERN-TH.6365 January 1992, Proc. Workshop on Physics at HERA, Hamburg, October 1991, ed. W. Buchmüller and G. Ingelman, to be published
- [3] J. Pumplin, Variables for distinguishing between quark jets and gluon jets, *in* Proc. 1990 DPF Snowmass Summer Study on High energy physics; *Phys. Rev.* D44 (1991) 2025; D45 (1992) 806
- [4] L. Lönnblad, C. Peterson and T. Rönvaldsson, *Phys. Rev. Lett.* 65 (1990) 1321; *Nucl. Phys.* B349 (1991) 675
- [5] L.M. Jones, *Phys. Rev.* D39 (1989) 2550; D42 (1990) 811
- [6] Z. Fodor, *Phys. Lett.* B263 (1991) 305;
I. Csabai, F. Czako and Z. Fodor *Nucl. Phys.* B374 (1992) 288
- [7] G. Barbagli, G. D’Agostini and D. Monaldi, Quark/gluon jet separation in the photoproduction region with a neural network algorithm *in* Proc. Workshop Physics at HERA (Oct 29–30, 1991), ed. W. Buchmüller and G. Ingelman
- [8] H. Baer, J. Ohnemus and D. Zeppenfeld, *Z. Phys.* C43 (1989) 675
- [9] P.D. Acton et al., *Z. Phys.* C53 (1992) 539;
S. Bethke and J. Pilcher, Tests of perturbative QCD at LEP, preprint EFI 92-14 (Feb. 1992) *Ann. Rev. Nucl. Part. Sci.*, to be published
- [10] G. Alexander et al. (OPAL Collaboration), *Phys. Lett.* B265 (1991) 462
- [11] M. Drees and K. Grassie, *Z. Phys.* C28 (1985) 451
- [12] F. Abe et al. (CDF Collaboration), *Phys. Rev. Lett.* 68 (1992) 1104;
F. Aversa et al., *Z. Phys.* C49 (1991) 459;
S. Ellis, Z. Kunst and D. Soper, *Phys. Rev. Lett.* 64 (1990) 2121
- [13] S. Hayward and N. Weiss, *Phys. Rev.* D45 (1992) 2360
- [14] M.A. Graham, L.M. Jones and P.R. Daumerie, Comparison of jet fragmentation schemes, Illinois University preprint ILL-TH-91-16-REV, November 1991
- [15] Y. Kim et al. (AMY Collaboration), *Phys. Rev. Lett.* 63 (1989) 1772
- [16] G. D’Agostini and D. Monaldi, Identification of high p_t jet events produced by a resolved photon at HERA, Proc. Workshop Physics at HERA (Oct 29-30, 1991) ed. W. Buchmüller and G. Ingelman